

# A high-brightness QCW pump source using a pre-aligned GRIN lens array with refractive beam correction

Roy McBride<sup>1a</sup>, Howard Baker<sup>a</sup>, Jean-Luc Neron<sup>b</sup>, Sead Doric<sup>b</sup>, Cristina Mariottini<sup>c</sup>, Enzo Nava<sup>c</sup>,  
Emanuele Stucchi<sup>c</sup>, Paolo Milanesi<sup>c</sup>

<sup>a</sup>PowerPhotonic Ltd, Earl Mountbatten Building, Riccarton Campus, Edinburgh EH14 4AS, UK;

<sup>b</sup>Doric Lenses Inc., 357 rue Franquet, Quebec QC, G1P 4N7 Canada

<sup>c</sup>Electro-optic section, CESI, via Rubattino 54, 20134, Milan, Italy

## ABSTRACT

We demonstrate a technique for collimating conduction-cooled QCW diode laser stacks that achieves very high brightness in a compact and robust package. First we collimate the bars in the fast-axis using a pre-aligned array of Doric™ GRIN cylindrical lenses, where each lens is oriented to correct the gross positioning errors of each bar. We then measure the residual beam errors using a proprietary wavefront mapping system, and fabricate a refractive wavefront correction phaseplate to effectively flatten the wavefront. The type of lens used exhibits particularly low aberration in the presence of misalignment, ensuring that the resultant wavefront can be effectively corrected. We applied the technique to two 0.5 mm pitch, 12-bar stacks operating at 1.2 kW. By this method, we repeatably obtained a 10-fold increase in stack brightness, reducing fast-axis beam divergence for the entire stack to below 0.3°, close to the theoretical limit. The result is an extremely compact, high brightness source optimised for side-pumping thin slab lasers.

**Keywords:** High power diode laser stack, high brightness, beam correction, collimation

## 1. INTRODUCTION

### 1.1 Application requirements

As part of a concept design study of a high-efficiency laser source for use in a space-based backscatter Lidar / DIAL instrument, we require a quasi-continuous wave (QCW) diode pump source for an Yb:YAG slab laser. The proposed laser is a side-pumped slab, where the pump light must be launched into an aperture of width >6mm and height <0.5mm. As part of this design study, we need to establish the limits to beam quality available from pump sources, in order to determine what freedom we have in other aspects of system design. As the application is for a space-based system, it essential that the source is light, compact, and very reliable.

### 1.2 Selection of stack

A detailed analysis of requirements for pump power and reliability led to the selection of a 12-bar conduction-cooled QCW stack, capable of operation at 1.2 kW peak power. These are widely available on nominal 500 μm bar pitch, providing the entire pump light within an area of 6 mm × 10 mm, as shown in Figure 1a. These stacks are widely used in military applications; hence their design is intrinsically robust, and well-suited to deployment in space.

Typical stack beam properties of this type of stack are slow-axis divergence of 10° FWHM (full width half maximum), fast-axis divergence 40° FWHM. 90% power of power is typically contained within 15° × 75° divergence.

While this large uncollimated divergence is acceptable for face pumping of thick slabs, collimation is required in order to produce the narrow stripe of pump radiation required for side pumping. These stacks are not, however, available from manufacturers as collimated units. It has therefore been necessary for us to develop a collimation process for this application.

---

<sup>1</sup> r.mcbride@powerphotonic.co.uk; phone +44 (0)131 451 3086; fax +44 (0)131 451 3088; [www.powerphotonic.com](http://www.powerphotonic.com)

## 2. PRIMARY COLLIMATION

### 2.1 Challenges of collimation

Fast-axis collimation of high-power diode laser (HPDL) stacks is straightforward when the pitch between bars is large (e.g.  $>1.5$  mm) and the fast-axis fill factor is low (e.g.  $\leq 50\%$ ). In our application, however, the small bar pitch and high fast-axis fill factor required make collimation a challenge.

Due to the stack geometry and beam properties, the collimation lenses must have effective focal length  $\sim 350$   $\mu\text{m}$  and diameter  $\sim 500$   $\mu\text{m}$ . The tight packing of the bars makes it difficult to align and fit these collimation lenses individually, for each bar, as there are only a few tens of microns clearance between lenses. One alternative is to fabricate an array of lenses mounted in the correct nominal location for each bar. However, the tolerance on separation of bars in the final stack can lead to cumulative deviations (Offset) of up to  $50$   $\mu\text{m}$  from the nominal position. This would result in bar-to-bar pointing errors of up to  $150$  mrad ( $8.5^\circ$ ), which is unacceptably high.

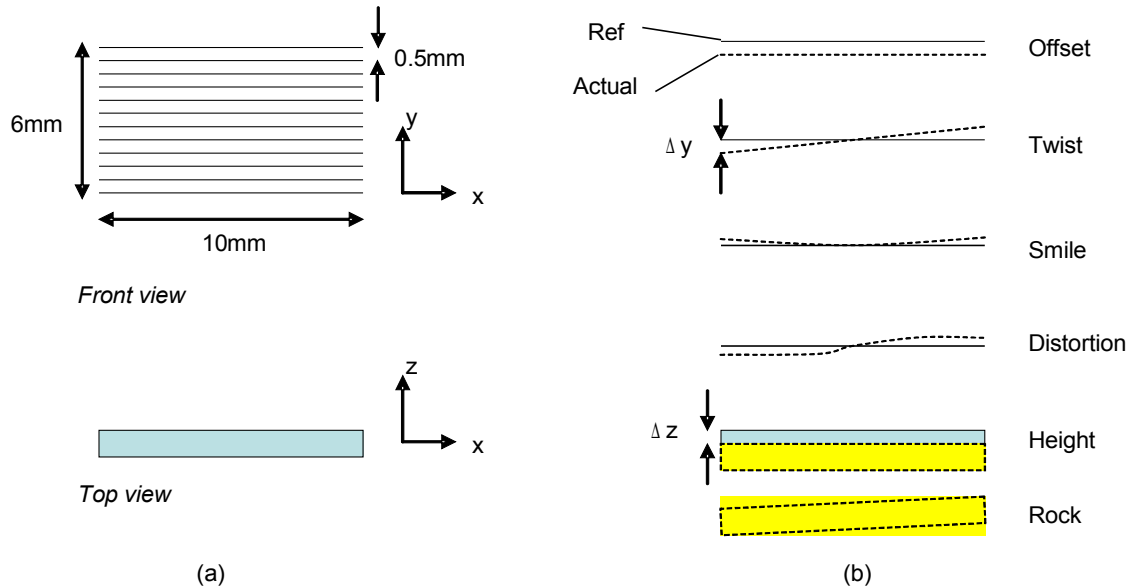


Fig. 1. Stack geometry, co-ordinate system and nomenclature (a) nominal stack geometry (b) deviations from nominal (reference) positions

The deviation in emitter position (in the fast axis) from its nominal position can also vary along the bar, as shown in Figure 1b. Bar Twist, Smile, and higher order Distortion all contribute to pointing errors, while Height and Rocking errors lead to defocus of the collimated beams, as illustrated in Figure 5a. Combined, these effects all increase the divergence and inhomogeneity of the collimated beam.

### 2.2 Collimation process: principle

Collimation errors due to translation and rotation of the bar (labeled as Offset, Twist, Height, and Rock in Figure 1b) can be avoided by fabricating a fixed array of lenses where the location and orientation of each lens corresponds to that of each individual bar. Provided emitter locations can be accurately measured, the resulting location data can be used to define locations for a V-groove pair for each collimator lens. This allows precise location of a collimating lens. Our design concept for such a lens mount is shown in Figure 2.

### 2.3 Selection of lens – mechanical and optical properties

Due to the high fast-axis divergence angle of HPDL emission, the key requirements for fast-axis collimation are low aberration and high numerical aperture, which typically leads to the selection of high-index acylindrical lenses. These give excellent performance when they can be aligned using all five degrees of freedom, and where misalignment and defocus errors are small. In our application, however, we rely on mechanical features to align the lens in roll (about its axis) and residual misalignments due to mechanical tolerances, bar smile and distortion are expected to be significant.

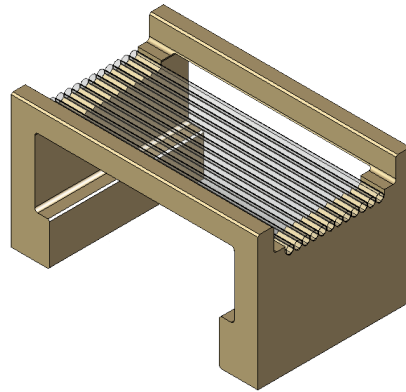


Fig. 2. Collimator assembly, based on precision-machined lens mount and Doric™ GRIN cylindrical lenses

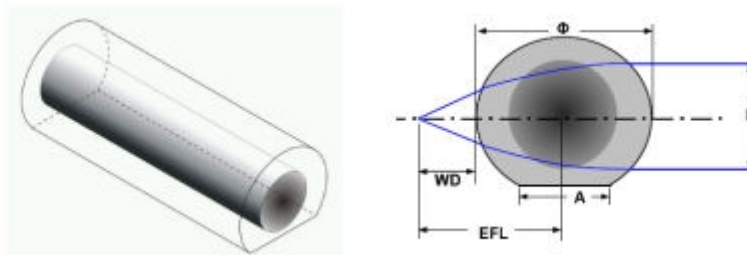


Fig. 3. Cylindrical GRIN collimation lens

For these reasons, we chose to use the Doric™ GRIN cylindrical lenses. Their cylindrical geometry (shown in Figure 3) allows precise location using a machined V-groove. Their intrinsic geometry makes them insensitive to misalignment by rotation about their own axis, and their Luneberg-lens properties result in low aberration when lateral misalignment is present (Offset, Twist, etc), a prediction that has been verified experimentally [1]. This is particularly useful when refractive optic beam correction is used for subsequent brightness restoration.

In this application we used Doric D148-392, which has an effective focal length (EFL) of 342  $\mu\text{m}$  and diameter of 500  $\mu\text{m}$ . These are fabricated with a flat on one side, which provides some extra space between lenses and increases freedom for alignment in the fast axis.

## 2.4 Implementation

We implemented this method of primary collimation on two stacks, both nominally-identical 0.5 mm pitch, 12-bar stacks operating at 1.2 kW, obtained from Nuvonyx Europe. Emission wavelength was 940 nm.

The actual location and shape of each bar were obtained by measuring emitter locations to  $\pm 1 \mu\text{m}$  using a travelling microscope. These V-grooves are defined in a single, rigid, copper frame, which is expansion-matched to the HPDL stack, as shown in Figure 2. This can then be aligned to the stack and fitted as a single optical element. The emitter locations are measured to an accuracy of  $\pm 1 \mu\text{m}$ , and the V-grooves are machined to a tolerance of  $< \pm 5 \mu\text{m}$ .

Zemax simulations based on the above tolerances and data gave a collimated fast axis divergence (90% power) of  $\sim 3^\circ$  (50 mrad). A complete lens mount, after fitting lenses and aligning to a stack, is shown in Figure 4.

A 90% power beam divergence of 50 mrad represents a factor of  $\sim 25$  improvement on the uncollimated stack. This would couple 90% of the power into an aperture of 500  $\mu\text{m}$  with an aberration-free F1.7 lens of focal length  $< 10\text{mm}$ . To couple power efficiently into a smaller aperture, or using a longer focal-length lens, requires better beam quality. This can be achieved by refractive-optic beam correction [2].

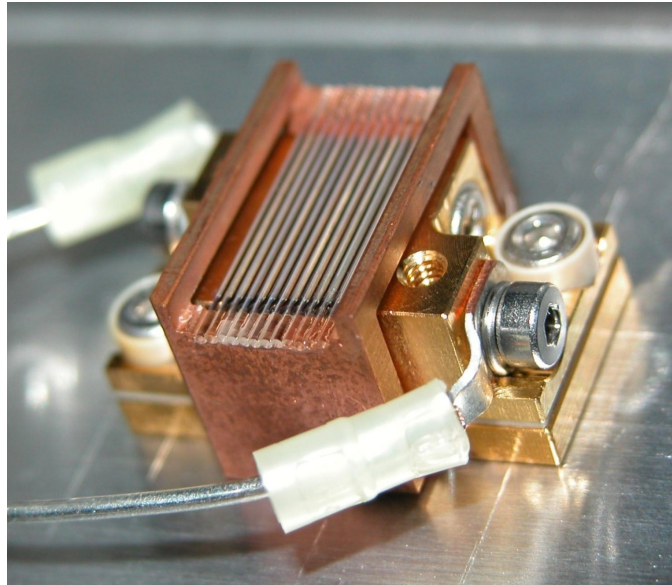


Fig. 4. Stack after primary collimation

### 3. BEAM CORRECTION

#### 3.1 Principles of beam correction

In practice, all collimated HPDL stacks suffer from imperfect collimation, due to emitter-lens misalignment and aberrations [3]. Misalignment, defocus, and aberration can all be considered as wavefront distortion relative to the ideal planar wavefront (Figure 5a). Such wavefront distortions can be corrected using a compensating refractive element - provided the first surface of this element is sufficiently close to the exit surface of the fast-axis collimator lens that the wavefront does not go through a caustic (ray crossing), as shown in Figure 5b.

The principle of refractive beam correction has already been demonstrated for continuous wave (CW) HPDL stacks with longer focal-length lenses and lower fill-factor [2]. The application we describe here places far more stringent demands on the technique than have been previously demonstrated, due to the high fast-axis fill-factor, small beam waist size, and large range of wavefront tilt present.

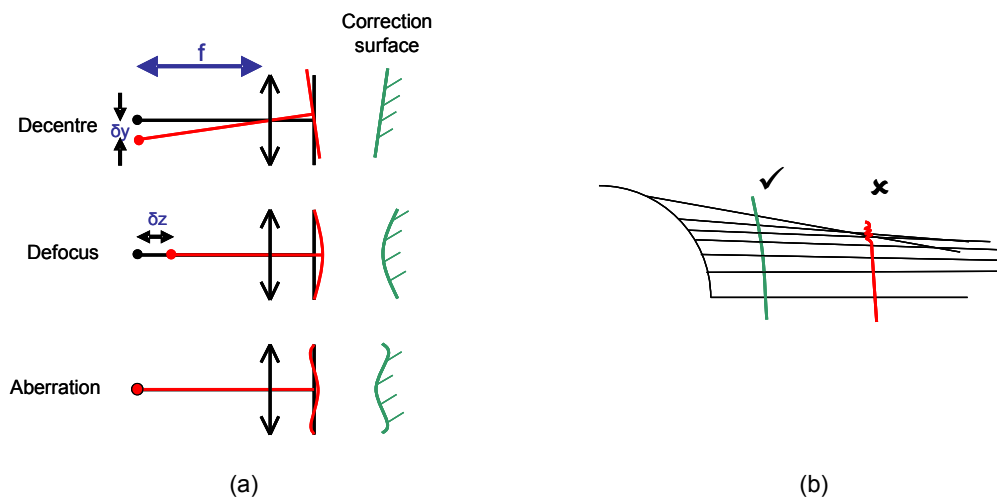


Fig. 5. a) Wavefront errors and their correction b) Correctable and uncorrectable regions of an aberrated wavefront

### 3.2 Implementation of beam correction

Design and implementation of beam correction followed the method reported in [2]. A map of wavefront tilt over a plane close to the fast-axis collimator (FAC) output surface was obtained using a proprietary measurement system based on the Hartmann technique [4]. These measurements were then numerically integrated as described in [4] to obtain the correction optical path difference (OPD) required to flatten the wavefront. From this we then obtained the appropriate refractive correction surface profile, assuming fused silica material.

Correction phaseplates were then laser-cut to this design in fused silica, and laser smoothed to provide a damage-resistant, low-scatter finish. The phaseplates were antireflection (AR) coated, then aligned and fitted to the lens mount using UV-curing adhesive.

## 4. RESULTS

### 4.1 Tests

We carried out the full primary collimation and correction procedure for both stacks.

Beam divergence was characterized using the setup shown in Figure 6. This arrangement allows an individual bar to be selected, and provides a separate fast-axis far-field pattern for each individual emitter in the bar. This allows pointing error and divergence to be visualized and quantified for each individual emitter in the stack. The resulting images can also be used to calculate overall divergence data for each bar. By removing the bar-selection slit, the entire stack can be characterized in a similar way.

To analyse the results, we calculated three beam divergence parameters:

- FWHM divergence, which is often used as guideline specification values
- 90% enclosed power divergence, an indicator of power coupled into a aperture and hence the most useful figure of merit for our application
- $4\sigma$  beam width, as defined in ISO11146 [5], used for calculation of resultant beam  $M^2$

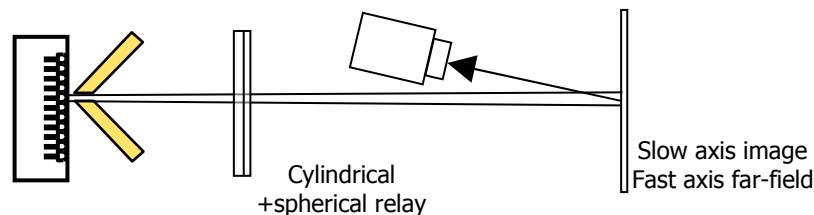


Fig. 6. Setup for emitter resolved pointing and divergence measurement

### 4.2 Results of collimation

Figure 7 shows images obtained using the setup shown in Figure 5 to characterize the individual bars of stack 2. Figure 9a shows an image obtained for the complete stack, with the bar-selector slit removed. Fast-axis divergence values calculated from these results are given in Table 1, where they are compared with nominal values for the uncollimated stacks.

Collimation reduced the headline FWHM divergence figure from  $\sim 40$  deg to  $\sim 1.4^\circ$  and  $1.1^\circ$  for the two stacks, respectively, i.e. approximately 30-40 $\times$  reduction in FWHM divergence. 90% power divergences were reduced from  $\sim 75$  deg to  $\sim 2.6^\circ$  and  $3.0^\circ$  (45 mrad and 53 mrad), respectively, reductions of  $\sim 25$ -30 $\times$ . These values are very close to the value of 50 mrad predicted by modeling, based on a 5  $\mu$ m lens positioning tolerance.

Comparison of these results shows that FWHM divergence is a poor indicator of 90% power divergence, since the ratio of FWHM divergence to 90% power divergence angle is not consistent between the two stacks. This is because 90% power is critically dependent on power distribution in the tails of the beam.

Considering our application, launching a beam of width 6 mm and divergence 53 mrad divergence ( $3.0^\circ$ ) into an aperture of 0.5 mm requires an aberration-free lens of focal length  $f < 10$  mm at F1.6. Launching this beam into an aperture below 0.32 mm requires a lens faster than F1. This level of collimation is therefore just capable of meeting requirements at the

edge of the possible specification range, but the consequent requirements on lenses are exacting, particularly if independent focusing of fast and slow axes is required in order to match the beam to the pump volume.

### 4.3 Residual errors for correction

The images for each individual bar, shown in Figure 7, illustrate the variety of residual collimation errors present. Each bar shows markedly different behaviour, vividly illustrating the effects of a few microns positioning error on collimation. Considering a few specific bars:

- In bar 2, the overall pointing is quite far from the mean of other bars, indicating a high Offset misalignment
- In bar 12, the lens is defocused, leading to high divergence, but is otherwise well-aligned
- In bar 3, the lens is well-focused at one end and defocused at the other (“Rock” in Figure 1), with a slight twist
- In bars 1, 4 and 5, the lens is well-focused in the centre, but defocused close to the ends (Rock)
- In all bars, pure U-shaped smile is relatively low, indicating a good packaging process, though in all bars there is a significant residual S-shaped smile-related distortion.
- In bar 7 in particular, each emitter is well collimated and smile is low, but the lens is twisted relative to the bar (rotated about the z-axis) and the bar is slightly distorted (“S”-shaped).

The low divergence of each emitter in bar 7, and in the well-focused regions of bars 1, 4 and 5 is noteworthy. For bar 7, while individual emitter pointing angles range over 50 mrad, there is no significant change to the individual emitter divergence. The far-field is free from the strong diffraction side lobes typical of a misaligned acylindrical lens. This result – low aberration in the presence of misalignment – is a particular feature of this type of collimation lens, and has important implications for beam correction. Low aberrations mean that the wavefront is well-behaved – the region close to the exit surface of the FAC lens is free from caustics (ray crossings), allowing wavefront correction to work well.

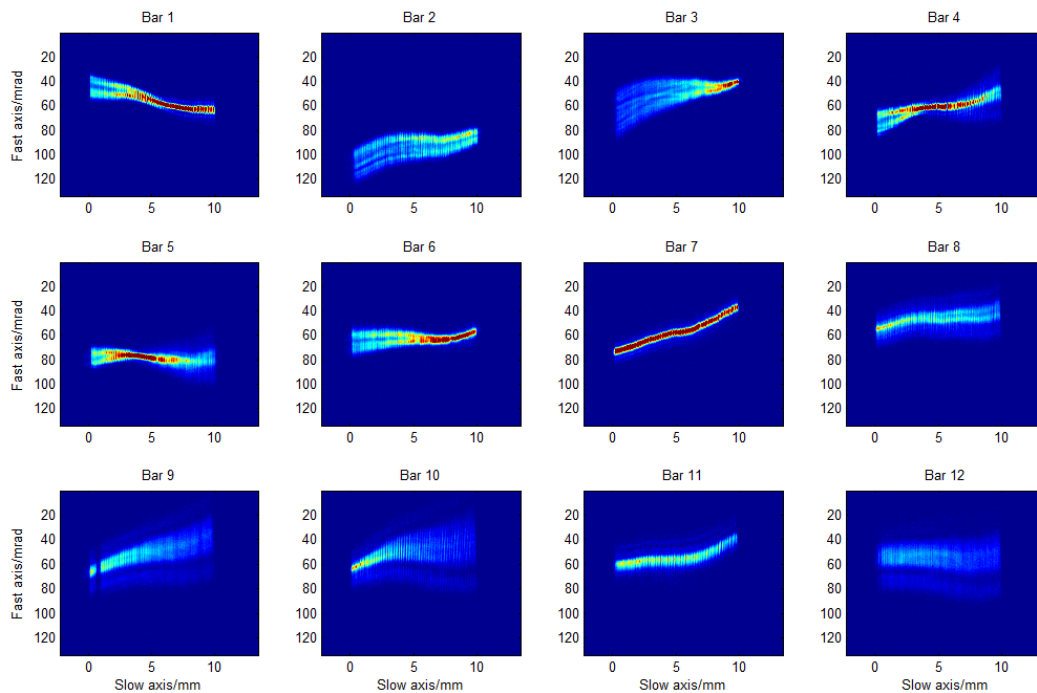


Fig. 7. Slow-axis resolved collimation errors for individual bars, after primary collimation

The overall divergence, shown in Figure 9a, therefore appears to be primarily due to errors that can be corrected. To estimate how far divergence could be improved (in principle) by correction, we compare the overall divergence to the theoretical ideal that would be obtained were each bar to be an independent Gaussian beam source, with perfect collimation (fast-axis  $M_f^2 = 1$ ) and perfect alignment.

To do this, we assumed a beam waist at the collimating lens. We obtained the near-field fast-axis intensity profile for individual bars from the measurement system used to characterize the wavefront, and calculated the second moment  $\sigma_{f0}$ . Following ISO 11146, the near-field beam waist diameter  $d_{\sigma f0}$  is then

$$d_{\sigma f0} = 4\sigma_{f0} \quad (1)$$

We obtained the far-field beam profile from the data plotted in Figure 8, and obtained the  $4\sigma$  beam divergence as

$$\theta_{\sigma f} = 4\sigma_f / z \quad (2)$$

We then calculated the effective per-bar fast-axis  $M_f^2$  as

$$M_f^2 = \frac{\pi}{\lambda} \frac{d_{\sigma f0} \theta_{\sigma f}}{4} \quad (3)$$

The results of primary collimation are shown in Table 1. Effective fast-axis per-bar  $M_f^2$  values for the two stacks were ~15 and 17. The true value of  $M_f^2$  for individual bars is better than this, since the overall effective  $M_f^2$  includes the effects of differences in pointing direction between bars.

	FWHM divergence		90% power divergence		4 $\sigma$ divergence		
	deg	mrad	deg	mrad	deg	mrad	M <sup>2</sup>
<b>Stack 1</b>							
Uncollimated (est.)	40	700	75	1310	-	-	-
Collimated	1.4	24.4	2.6	45.0	3.13	54.67	14.9
<i>Improvement factor</i>	29		29		-		
<b>Stack 2</b>							
Uncollimated (est.)	40	700	75	1310	-		
Collimated	1.1	18.4	3.0	53.1	3.65	63.68	17.4
<i>Improvement factor</i>	38		25		-		

Table 1. Results of primary collimation. Near-field beam waist diameter  $d_{\sigma f0} = 326 \mu\text{m}$  for both stacks

In practice, achieving  $M_f^2 = 1$  is not possible – the beams are not infinite Gaussians, they are non-Gaussian and truncated. The useful numerical aperture of the FAC lenses is specified 0.50, hence extreme rays will suffer from aberration. Finally, rays that are not paraxial in the slow axis will see a different focal length at the FAC (the “bow-tie” effect) – hence perfect collimation cannot be achieved simultaneously for all rays within the slow-axis divergence range.

Typically, these effects limit the achievable  $M_f^2$  to 1.2 - 1.5. In this case, this opens the possibility of a further factor of 10-fold improvement in divergence over the primary-collimated beam.

#### 4.4 Results of wavefront correction

The map of calculated correction OPD for stack 2, derived from our wavefront measurement, is shown in figure 8. Overall correction OPD range was around 20  $\mu\text{m}$ , requiring a correction surface with a sag of approximately 40  $\mu\text{m}$ . The individual bar correction surfaces of figure 8 can be related directly to the images of figure 7. For example, the Twist misalignment present in most bars leads to a twisted correction surface, while the strong Offset in bar 2 results in a steeply-sloping correction surface.

The divergence image after wavefront correction is shown in Figure 9b and the derived divergence values are tabulated in Table 2. The image shows the further dramatic improvement in beam quality achieved by wavefront correction. All emitters are now co-aligned and have low divergence. Pointing errors due to Offset, Twist, Smile and Distortion have been effectively removed, and divergence increase due to Height and Rock defocus errors has also been removed.

Figure 10a provides a direct comparison of the uncorrected and corrected divergence profiles both directly and expressed as a power in the bucket (PITB, or integrated power) curve. Correction transforms a broad, unstructured divergence profile into a clean, Gaussian-like profile with a narrow central lobe and low power in the tails of the beam.

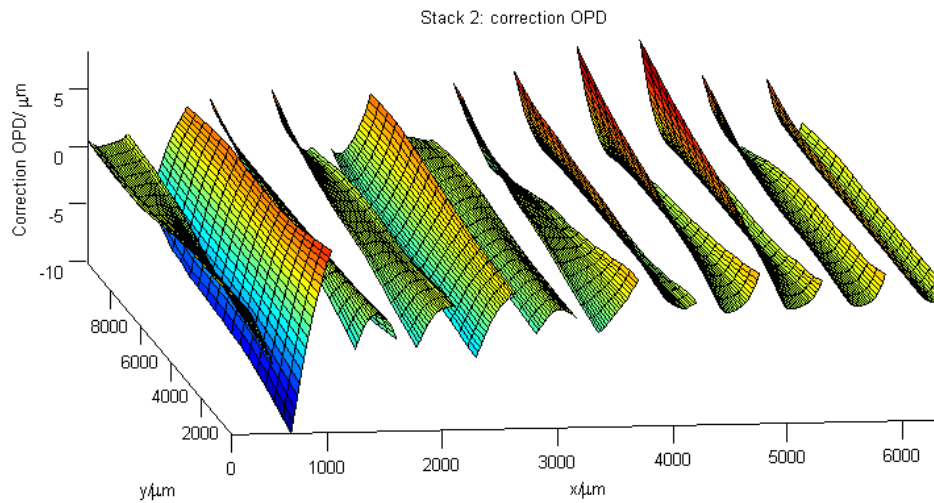


Fig. 8. Calculated OPD correction for stack 2.

Improvements in  $4\sigma$  divergence and  $M_f^2$ , shown in Table 2, are factors of 9.3 and 10.1 for the two stacks. Improvement factors for the critical 90% divergence figure are 9.4 and 10.3, respectively – i.e. the overall divergence improvement over primary collimation is roughly a factor of 10, by both measures. The resultant effective bar  $M_f^2$  values of 1.6 and 1.7 show that there is very little further improvement in divergence possible by further correction and realignment of beams. After correction, mean 90% power divergence over both stacks is around 5 mrad ( $<0.3^\circ$ ). This provides far greater freedom in the design of the pump module, and selection of slab dimensions, than the  $\sim 50$  mrad ( $3^\circ$ ) value obtained by primary collimation alone.

A separate measurement was carried out to ensure that correction had no negative impact on the slow-axis divergence. Slow-axis divergence profiles were obtained and compared, and it was verified that wavefront correction had no measurable effect on the slow-axis divergence.

	90% power divergence		4 $\sigma$ divergence		
	deg	mrad	deg	mrad	M <sup>2</sup>
<b>Stack 1</b>					
Collimated	2.58	45.0	3.13	54.67	14.9
Corrected	0.28	4.81	0.34	5.89	1.60
<i>Improvement factor</i>	9.4		9.3		
<b>Stack 2</b>					
Collimated	3.04	53.1	3.65	63.68	17.36
Corrected	0.30	5.18	0.36	6.29	1.71
<i>Improvement factor</i>	10.3		10.1		

Table 2. Results of beam correction. Near-field beam waist diameter  $d_{\sigma f0} = 326 \mu\text{m}$  for both stacks

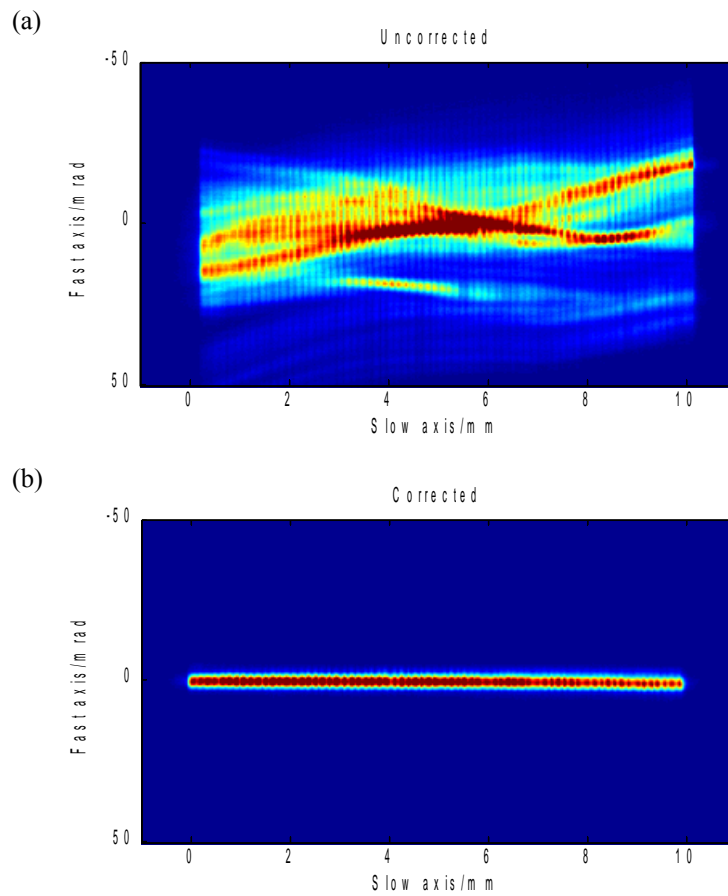


Fig. 9. Slow-axis resolved collimation errors for entire stack (stack 2), uncorrected (collimated) and corrected

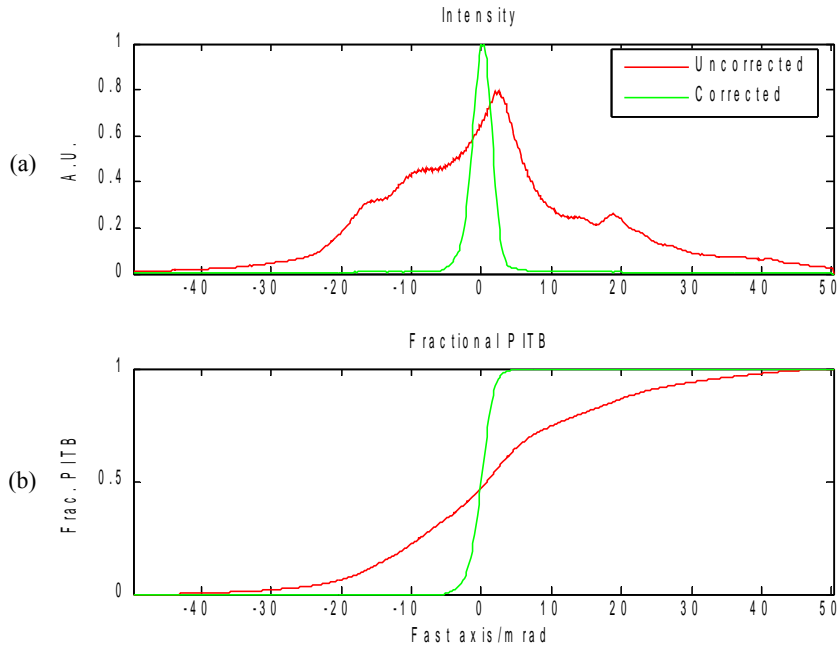


Fig. 10. Fast axis divergence plots for stack 2, before and after correction: (a) divergence profile (Intensity) (b) cumulative power profile (PITB, power in the bucket)

## 5. CONCLUSIONS

We have developed a method for high beam-quality collimation of small-pitch conductively cooled QCW diode laser stacks, and have demonstrated the method by applying it to two stacks. High performance was achieved by carrying out collimation in two stages:

In the first stage, we assembled a pre-aligned array of Doric™ GRIN cylindrical lenses, where the location of each lens was defined by a precisely-machined lens holder, based on a measurement of emitter positions. The entire lens array was then aligned to the stack as a single collimating element. The residual collimation errors can be attributed to bar smile and distortion, and to micron-scale tolerances in fabrication of the lens holder. This provided a worst-case 90% divergence of  $3.0^\circ$  (53 mrad) – roughly  $25\times$  lower than the uncollimated beam.

In the second stage, we further increased the brightness of the stack by characterising the residual wavefront errors in the fast-axis direction, then fabricating a custom refractive phaseplate to correct these errors. By this method, we further reduced 90% power divergence angle by a factor of 10, to 5 mrad. ( $<0.3^\circ$ ). This fast-axis beam divergence is equivalent to a stack with all emitters perfectly co-aligned (i.e. no twist or smile), each collimated with fast-axis  $M^2 < 1.7$ , which is close to the practical limits imposed by the combination of diffraction and the bow-tie effect. The fact that Doric grn cylindrical lenses are least sensitive to defocus and tilt played a crucial role in the success of the stack collimation and prepared good initial conditions for subsequent phaseplate correction of the beam.

We have thus realised an extremely compact high-brightness source whose beam is perfectly suited to side-pumping of thin slab lasers.

**Acknowledgement:** This work was carried out under ESA/ESTEC CONTRACT N. 18949. “High efficient Laser Pump Source for LIDAR Applications”

## REFERENCES

- <sup>1</sup> Holdsworth A R, Baker H J “Assessment of micro-lenses for diode bar collimation” Laser Diode and LED Applications III, San Jose 1997, ed. K Linden, SPIE Proceedings 3000, 209-214 (1997)
- <sup>2</sup> J. F. Monjardin, K. M. Nowak, H. J. Baker, and D. R. Hall, “Correction of beam errors in high power laser diode bars and stacks” Opt. Express **14(18)**, 8178- 8183 (2006)
- <sup>3</sup> U. Brauch, P. Loosen, and H. Opower, “High-power diode lasers for direct applications,” in High Power Diode Lasers, R. Diehl, ed., (Springer-Verlag Berlin Heidelberg, 2000), pp. 303-368.
- <sup>4</sup> I. Ghozeil, “Hartmann and other screen tests,” in Optical Shop Testing, D. Malacara, ed., (Wiley, 1992), pp. 367-396.
- <sup>5</sup> EN ISO 11146-1:2005 Lasers and laser-related equipment - Test methods for laser beam widths, divergence angles and beam propagation ratios - Part 1: Stigmatic and simple astigmatic beams